Please do not adjust margins

# Decomposition mechanism and morphological evolution of *in-situ* realized Cu nanoparticles in Cu complex inks

Received 00th January 20xx,
Accepted 00th January 20xx

DOI: 10.1039/x0xx00000x

Nihesh Mohan*[a], Juan Ignacio Ahuir-Torres [b], Sri Krishna Bhogaraju[a], Ralf Webler[c], Hiren Kotadia[b], Huseyin Erdogan[d] and Gordon Elger [a]

Cu complex inks are composed of Cu salts as metal precursors and complexing agents that effectively reduce the decomposition temperature of the Cu salts. The thermal decomposition of the complexed Cu salt provides the metal for the in-situ formation of nanoparticles. Using Cu formate tetrahydrate as metal precursor, the effect of complexing agent, i.e. amino-2-propanol and hexylamine, its molar ratio compared to the Cu salt, the predrying and sintering parameters, i.e. temperature and ramp rate, and additional organics solvents are investigated to understand the influence on morphology of *in-situ* generated Cu nanoparticles. The additional solvents are used to adjust the viscosity for ink-jet printing and to control the formation of the nanoparticles. A pre-drying step with slow ramp rate (5°C/ min) is required before the sintering process to effectively control the evaporation of organics. However, the slow pre-drying process lead to the growth of in-situ genrated particles into the microscale range (2-5 µm). Adding Polyethylene glycol 600 (PEG600) is observed to supress the growth of nanoparticles and realize an ink-jet printable formulation, which achieves even with low Cu content (< 8 wt.%), dense and homogeneous traces with a bulk resistivity of 20.48 µΩcm when sintered in a conventional oven for 5 min at 250°C under a $N_2$ atmosphere.

## Introduction

Printed electronics involves printing or deposition of innovative functional materials such as metal conductive inks onto suitable substrate to connect and assemble microelectronic devices.[1-2] The growing demand for printed electronics in areas such as flexible electronics, smart Radio-frequency identification (RFID) components, energy harvesting and storage devices, thin film transistors, display technology, wearable sensors for health monitoring applications and many others, is due to its lower operational costs, good scalability, and energy efficient solutions.[3-8]

In the realm of printed electronics, the conductive trace serves as a crucial component where particle sintering plays a vital role.[9] In recent years, there has been rapid development and commercialisation of metal nanoparticles (NPs) based inks owing to its relatively high metal loading content (~ 50 metal wt.%) and good electrical conductivity.[10] Ag NPs inks have been successfully introduced for manufacturing in the field of printed electronics in the last 15 years.[11-12] But owing to the high cost of Ag NPs inks, Cu based NPs inks are investigated as a low-cost alternative for forming conductive traces.[13-15] There are several commercially available Cu NPs inks. However, these inks have a complex synthesis route and issues with nozzle clogging in printing systems due to inhomogeneous particle size distribution and/or agglomeration. Further, the inks need deep-freeze or refrigerated storage conditions, which leads to a shorter shelf life and reduced usability.[16]

[a] Institute of Innovative Mobility, Technische Hochschule Ingolstadt, Esplanade 10, 85049, Ingolstadt, Germany.
[b] School of Engineering, Liverpool John Moores University, Liverpool, L3 3AF, UK
[c] Schlenk SE, Barnsdorfer Hauptstrasse 5, 91154 Roth-Barnsdorf, Germany
[d] Conti Temic microelectronic GmbH, Ringlerstrasse 17, 85057 Ingolstadt, Germany

The inclusion of anti-agglomerates and passivation layers in the ink formulation results in higher sintering temperatures (>200°C) due to the high boiling point and/or thermal decomposition temperature of such additives. Further, the typical reported sintering times are 30-60 minutes.[17] Therefore, there is a growing interest in the development of Cu complex inks as an alternative solution, with the goal to achieve shorter sintering times, even with conventional sintering processes and lower sintering temperatures (<150°C).[18-20]

Cu complex inks provide a facile, low-cost alternative to Cu NPs inks for printed electronics application. The inks can be referred to as particle free since the salt is dissolved in the complexing medium and exists in the ionic form. Agglomeration during storage and oxidation at ambient temperature is hence avoided.[21] Compared to conventional NPs inks, Cu NPs form during the thermal decomposition of Cu salts. Cu complex inks, widely reported to have lower sintering temperature compared to NPs inks, are formed by mixing Cu salts, which act as a Cu metal precursor, with complexing agents that support dissolving the Cu salts and decrease the thermal decomposition temperature and solvents that help in improving the rheological properties of the ink. [18, 22-23] In addition, organics can be introduced for further size and shape control of the in-situ realized NPs. However, these inks have high organic content (> 85%) and efficient degassing of organics is required during the sintering process to prevent trace heterogeneities and voids which lead to poor conductivity.[24] A pre-drying step together with a slow ramp rate during the sintering process has previously shown to effectively control the rapid evaporation from the printed traces to form conductive Cu traces when following a conventional oven curing process.[25] Nevertheless, it is observed that after the slower ramp rate, the aggregation of *in-situ* formed Cu NPs lead to formation of larger particles in the range of 2-5 µm.[25,26] As a consequence, sparsely distributed metallic traces with lower electrical conductivity are obtained.

Please do not adjust margins

Please do not adjust margins



**Table 1** A brief summary of state of the art in Cu complex inks

| *S.No.* | *Cu precursor* | *Complexing agent* | *Solvent* | *Substrate* | *Fabrication method* | *Sintering condition* | *Resistivity (μΩcm)* | *Ref.* |
|---|---|---|---|---|---|---|---|---|
| 1. | Cu (II) formate tetrahydrate | Hexylamine | | Glass | Squeegee Coating | 250°C for 2 min, formic acid | 5.2 | 27 |
| 2. | Cu (II) hydroxide | Formic acid & citric acid in $NH_4OH$ | 2-methoxyethanol, ethylene glycol & polyvinylpyrrolidone (PVP) | PET, Polyimide | Handwritten using pen | Intense pulse light sintering (40-60 J/cm²) | 3.21-5.27 | 28 |
| 3. | Cu (II) formate tetrahydrate | Hexylamine | | Glass | Squeegee coating | 140°C for 30 min, $N_2$ | 9.6 | 29 |
| 4. | Cu formate | Dipropylene glycol monomethyl ether | Disperbyk 180, distilled water | Glass | Screen printing | 170°C-250°C for 30 min with $N_2$ | 3.29 | 30 |
| 5. | Cu (II) formate tetrahydrate | Octylamine, Butylamine | Ethanol | Glass | Drop deposition | 200°C for 40 min | 4.28 | 31 |
| 6. | Anhydrous Cu formate | Amino-2-methyl-1-propanol | Diethylene glycol monomethyl ether, n-pentanol, PVP | Polymeric substrates | Inkjet printing | Plasma curing (200 W, 40kHz, 0.2 mbar), $N_2$, 15 mins | 2.38 | 32 |
| 7. | Cu plates as electrodes | Formic acid, acetic acid, $NH_4OH$ | Ethanol, trimethoxysilane | Polyimide | Inkjet printing | Intense pulse light sintering (2000kW, 12 ms) | 2.3 | 33 |
| 8. | Cu (II) formate tetrahydrate | 3-Butylpyridine, Dipropylamine | Tetrahydrofuran | Glass | Drop deposition | 100°C for 30 min under $N_2$ | 8 | 34 |
| 9. | Cu (II) formate tetrahydrate | Butylamine, pentylamine (PA), hexylamine, octylamine | | Glass | Mask printing | 100°C-120°C for 30 min, $N_2$ | 5.7 | 35 |
| 10. | Copper formate | $NH_4OH$, dimethylamine | Dimethyl sulfoxide | Glass, PET | Inkjet printing | 120°C on hot plate under air (ramp rate: 5°C/min) | 0.05 ohms/sq | 36 |

*In-situ* control of particle size of Cu nanoparticles in Cu complex ink is thus required, with the goal to generate fine but uniformly distributed NPs that provide a dense and homogenous trace. Table 1 gives a brief summary of state of the art in Cu complex inks. The literature provides an insight into various Cu complex inks investigated with focus on results with lower bulk resistivities (<10 μΩcm), shorter sintering time and possible sintering under air. However, the influence of sinter ramp rate and solvent on *in-situ* particle formation and sintering can be further extensively discussed.

NPs are formed through assembly or interaction of ionic, atomic, or molecular units through various thermo-chemical reaction processes to form sub-nano structure.[37] By controlling these thermo-chemical reactions, it is possible to control the nucleation, growth, and morphology of NPs.[37-38] While previous publications have discussed the morphology control of Cu NPs with focus on synthesis methodology and influence of capping agents, factors influencing the morphology of in-situ generated Cu NPs in inkjet printable Cu complex inks have not been investigated extensively.[39-41]

This scientific study evaluates different approaches to control the size of *in-situ* generated Cu NPs. Cu(II) formate tetrahydrate is used as Cu precursor. Unlike Cu NP inks, there is no capping agent and/or anti-agglomerate, but an amine ligand is coordinated to Cu(II) formate for *in-situ* generation of Cu NPs. Both ink chemistry of the inks and sintering parameters are varied to study their influence individually. In addition, the role of carrier solvents with and without a particle size controlling binder (PEG 600) is also investigated.

## Experimental

**Materials**

Cu (II) formate tetrahydrate (Cuf), (98%) was purchased from Thermo Fischer Scientific. Amino-2-propanol (A2P) (93%) and Hexylamine (HA) (99%) were all purchased from Sigma-Aldrich. Ethanol (>96%), ethylene glycol (EG) (>99%) and Polyethylene glycol 600 (PEG 600) were purchased from Carl Roth. Polyimide films (Kapton® HPPST-125 μm) from DuPont were used for printing. Apart from Cuf and polyimide film, other chemicals were used as received.

**Synthesis**

Firstly, the decomposition behaviour of Cuf was analysed in two forms: as received (hydrated) and predried form (PCuf). In both cases, the salt was crushed manually for 15 minutes in a ceramic crucible. The predrying was done under air at 120°C for 15 mins on a hot plate. After evaluation, solely Cuf was used for all further detailed investigations. Next, two Cuf complexes were prepared using HA and



This journal is © The Royal Society of Chemistry 20xx

Please do not adjust margins

A2P. Cuf-HA (mixed in molar ratio of 1:1) and Cuf-A2P (mixed in molar ratio of 1:2) were prepared. Following the evaluation, only Cuf-A2P complex was pursued for investigating the influence of mixing molar ratio on complex decomposition and particle formation. Three Cuf-A2P complexes (mixed in molar ratio of 1:1, 1:2 and 1:3) were prepared. Based on the investigations, Cuf-A2P (1:2) complex was selected to realize printable ink formulations since it ensures the optimal complexing of all Cuf. Ink 1 and Ink 2 were prepared using different solvent combinations, e.g., ethanol, EG and PEG 600, to adjust the viscosity in the range of 10-12 mPa.s, essential for ink-jet printing.[42] Table 2 shows a detailed synthesis of the two Cu complex inks prepared for this scientific study. The viscosity of the inks was measured using a viscometer (Thermo Scientific Haake ™ Viscotester ™) and the contact angle of the inks on polyimide substrate were measured using a drop shape analyser (Kruss DSA 30M).

**Table 2** Detailed synthesis of Ink 1 and Ink 2 indicating the mass (in wt. %) of Cuf, A2P and carrier solvent, Cu metal content (in wt. %) and viscosity

| Cu complex inks | Ink 1 | | | Ink 2 | | |
|---|---|---|---|---|---|---|
| Cu precursor | Cuf | | | Cuf | | |
| Complexing agent | A2P | | | A2P | | |
| Molar ratio (Cuf:A2P) | 1:2 | | | 1:2 | | |
| Carrier solvent (with mixing mass %) | Ethanol (75%) + EG (25%) | | | Ethanol (99%) + PEG 600 (1%) | | |
| Mass (in wt.%) of Cuf, A2P and carrier solvent (CS) | Cuf | A2P | CS | Cuf | A2P | CS |
| | 24 | 16 | 60 | 30 | 20 | 50 |
| Cu metal content (in wt.%) | 6.768 | | | 8.46 | | |
| Viscosity (mPa.s) | 12 mPa.s | | | 9.5 mPa.s | | |

**Printing and Processing**

The Cu complex inks were printed using a Dimatix Materials Printer (DMP-2850, Fujifilm Dimatix Inc.) onto the polyimide substrates. Before printing, Ar-plasma treatment of the polyimide substrates was done for 5 minutes to remove organic residues from the surface. The Ar-plasma treatment was done using Zepto PLS from Diener electronic under UV in a manually controlled Ar atmosphere. After printing, a two-step pre-drying and sintering process is conducted in a reflow oven (UniTemp RSS 160-S) under a constant $N_2$ flow of 5l/min. The pre-drying is performed at 100°C for 5 min followed by a sintering step at 250°C for 5 min.

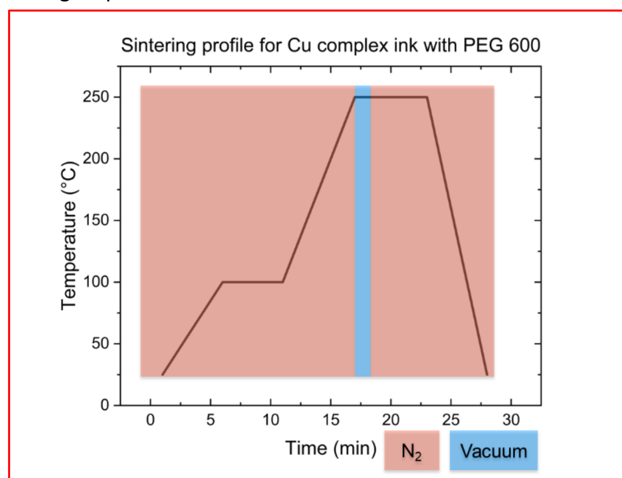


**Fig. 1** Sintering profile for the Cu complex ink With PEG 600

Fig. 1 shows the sintering profile for the Cu complex ink used in this study. Additionally, to facilitate efficient removal of PEG 600 from the system, a vacuum process was integrated at 250°C for 1 minute, enhancing the sinterability between the formed particles (as shown in Fig.1).

**Characterization**

The thermal decomposition behaviour of both the inks and their individual constituents was analysed by differential scanning calorimetry (DS C821 Mettler Toledo). The measurements were conducted under $N_2$ atmosphere with a flow rate of 30 ml/min, and the heating rate was set at 10°C/min. The analysis included heating the samples up to 250°C, followed by an isothermal step at 250°C for 5 minutes. Similarly, thermal gravimetric analysis (TGA) and differential thermal analysis (DTA) was conducted on Mettler Toledo TGA/DSC 3+ at the heating rate of 10°C/min under $N_2$ with 30 mL/min flow rate. The particle morphology after sintering was evaluated using a scanning electron microscope (Zeiss Auriga 40 Crossbeam FIB/SEM) with following parameters (Electron High Tension: 3 KV, Working Distance: 5.6 mm, Mode: Secondary Electrons). The thickness **(t)** of the trace was measured using an optical light profilometer (Nanofocus µ-surf custom) and sheet resistance ($\boldsymbol{R_s}$) measured using a 4-point probe (Keithley 2461). The bulk resistance ($\boldsymbol{\rho}$), thereafter is calculated using the following equation:[43]

$$\boldsymbol{\rho = t * R_s} \tag{1}$$

## Results and discussion

**Decomposition mechanism and characterization of Cu (II) formate tetrahydrate and its complexes**

The thermal decomposition of Cuf and resulting by-products are mentioned in equation 2 & 3.[44-46]

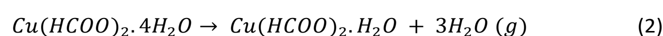

$$Cu(HCOO)_2.4H_2O \rightarrow Cu(HCOO)_2.H_2O + 3H_2O\ (g) \tag{2}$$

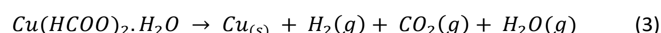

$$Cu(HCOO)_2.H_2O \rightarrow Cu_{(s)} + H_2(g) + CO_2(g) + H_2O(g) \tag{3}$$

The decomposition of Cuf has been extensively reported showing a two-step weight loss process, whereas decomposition of PCuf is a one step process.[44-46] In case of Cuf, the first weight loss is attributed to the dehydration of the tetrahydrate, as anticipated, while the second weight loss is caused by the decomposition of anhydrous Cu formate into metallic Cu.[44-46] Experimental investigations were conducted to examine the variations in the decomposition behaviour between Cuf and PCuf. The DSC and TGA analysis revealed the following observations (see Fig. 2.a and 2.b). Firstly, evaporation of water of hydration commences at room temperature and concludes at 104°C for Cuf. The endothermic peaks observed at temperatures of 52°C, 80°C, and 102°C correspond to the removal of the first, second, and third water of hydration, respectively.[45-46]

Theoretical and experimental mass calculations (using TGA) reveal that the expected mass change after removing three water molecules of hydration in Cuf is approximately 75%. TGA results show, after the first mass loss step (confirming removal of three waters of hydration as indicated by DSC), the experimental mass change at 125°C is about 74 ± 1%. This suggests the presence of a fourth water molecule of hydration in the Cuf crystal. Furthermore,

This journal is © The Royal Society of Chemistry 20xx

Please do not adjust margins



the theoretical and experimental calculation of Cu metal content in wt.% (shown in Table 3) indicates the absence of water of hydration in the case of PCuf.

Table 3 Theoretical and experimental Cu metal content (in wt.%) for Cuf and PCuf.

| Cu metal content after decomposition | Cuf | PCuf |
| --- | --- | --- |
| Theoretical Cu metal content (wt. %) | 28 | 41 |
| Experimental Cu metal content (wt. %) | 30±1 | 41±1 |

According to the literature, water in Cu (II) formate is held in place by hydrogen bonds between the relatively stable Cu and format ions.[47] Dehydration causes minimal misalignment between Cu and format ions, suggesting a good fit across the interface.[47-48] Consequently, after dehydration, the layers only experience slight relaxation, and any remaining water molecules must diffuse through the anhydrous lattice to escape.[47] In the dehydration process of Cu (II) formate tetrahydrate, the slow step is believed to be the diffusion of water molecules from the hydrate into adjacent sites of anhydride lattices at the interface.[47] Water retained at these sites may affect surface equilibria, potentially reducing the dissociation rate (forward reaction) and promoting the back reaction, leading to the recrystallization of metastable water-depleted hydrate.[47-48] This process could result in larger and more perfect crystals during the product phase, with wider channels in the recrystallized lattices aiding the escape of remaining water.[47-48]

Additionally, after pre-drying PCuf at 120°C for 15 minutes, grinding occurred due to the recrystallization of the salt, forming larger crystals. This suggests that the fourth water of hydration assists in the recrystallization process during pre-drying and is absent in the TGA measurement of PCuf. In contrast, Cuf, subjected to a rapid heating rate of 10°C/min in DSC, did not allow sufficient time for generating large crystals, leading to the observation of the fourth water of hydration in the TGA measurement of Cuf. The crystal size is proportional to the drying time and inversely proportional to the heating rate.

Consequently, three water of hydration molecules are eliminated, resulting in the formation of $Cu(HCOO)_2.H_2O$ (See Fig 2.g).[45-46] Decomposition of formate group is observed by an exothermic peak at 217°C for Cuf and at 224°C for PCuf showing release of $CO_2$, $H_2$ and $H_2O$ gas. From the TGA results, it is observed that the total mass loss was completed at 235°C (70 % mass loss) and 250°C (59 % mass loss) for Cuf and PCuf respectively. Although the exothermic peaks are very close between Cuf (217°C) and PCuf (224°C), the latter took longer to complete the thermal decomposition process (See Fig 2.a & 2.b). This can be attributed to the 4$^{th}$ water of hydration acting as a catalysing agent in the formate decomposition process of Cuf. [18]

The 4th water of hydration in Cuf generates intermediate exothermic reactions with the Cu formate (see Fig. 2.g).[49] These exothermic reactions generate temperature increase that accelerate the decomposition reaction in case of Cuf. The 4th water of hydration also supports the breaking of the chemical bond between Cu and formate group. The water of hydration can bond with the Cu, producing the instability of the Cu formate chemical bond due to Cu having an electron excess.[49] As seen in the figure above, the water of hydration is regenerated during the reaction as a byproduct. Therefore, the water of hydration is not consumed for this chemical reaction, thus it acts as a catalyst. A similar observation was made, where it was found that coordinated water in hydrated complex acts as a catalysing agent in the formate decomposition process.[18] A notable feature is that these catalysing agents encourage the electron localisations that prompts the chemical reaction . Fig. 2.c and 2.d show the SEM images for Cuf and PCuf after thermal decomposition at 250°C under N2 without any isothermal holding time at 250°C to prevent further sintering of the particles. The particle sizes calculated for Cuf and PCuf using the Image J software are 429.93 ± 101 nm and 378.07 ± 88 nm respectively (Fig. 2.e). Based on the particle size distribution curve, it can be seen that particle size in case of Cuf is slightly larger than PCuf owing to lower decomposition temperature of Cuf. As decomposition occurs earlier, the nucleation and growth process start earlier in case of Cuf compared to PCuf resulting in slightly larger particles in case of Cuf.

Based on these experiments, Cuf was selected as Cu precursor. Cuf was added to two different amine-based complexing agents: A2P (alkanolamine) and HA (alkylamine). The two complexing agents have different boiling points (HA-131°C and A2P-159°C) influencing their removal rate. The complex decomposition starts by decarboxylation (formate oxidation) and Cu reduction reaction (formation of Cu particles), where CO2 and H2O are released as by-products indicated by an exothermic reaction.31 This is followed by the release of amine ligands indicated by an endothermic reaction. The decarboxylation reaction marks the onset of Cu reduction process ($Cu^{2+}$ → $Cu^{1+}$ →$Cu^0$) which provides the temperature window in which Cu0 forms, nucleates, and grows into particles.50 In Fig 3.a, it can be seen that Cuf-A2P has a narrower exothermic peak at 143°C compared to Cuf-HA at 137°C, which indicates a higher nucleation rate leading to formation of smaller particles with narrow size distribution.50 This is also confirmed by the SEM images of Cuf-HA and Cuf-A2P after decomposition at 160°C under N2 (as seen in Fig. 3.b and Fig. 3.c respectively). During the nucleation and growth phase, the smaller particles tend to grow either by one of the two mechanisms Coalescence or Ostwald ripening resulting in larger particles.52 In case of Cuf-HA, the nucleation rate is slower compared to Cuf-A2P as observed from Fig. 3.a – where a broader exothermic peak is observed. From Fig. 3.b and Fig. 3.c, it can be seen that particles have dissimilar sizes after decomposition for Cuf-HA compared to Cuf-A2P at 160°C. This can be explained due to the slower nucleation and longer growth phase in case of Cuf-HA. Additionally, as the temperature increases - the released amine ligands evaporates earlier in case of Cuf-HA (~165°C) compared to Cuf-A2P (~180°C). This allows the formed particles to come in contact earlier and form sinter necks which eventually grows as the temperature and time increases until a steady sintering state is reached.[53]


This journal is © The Royal Society of Chemistry 20xx

Please do not adjust margins

Please do not adjust margins



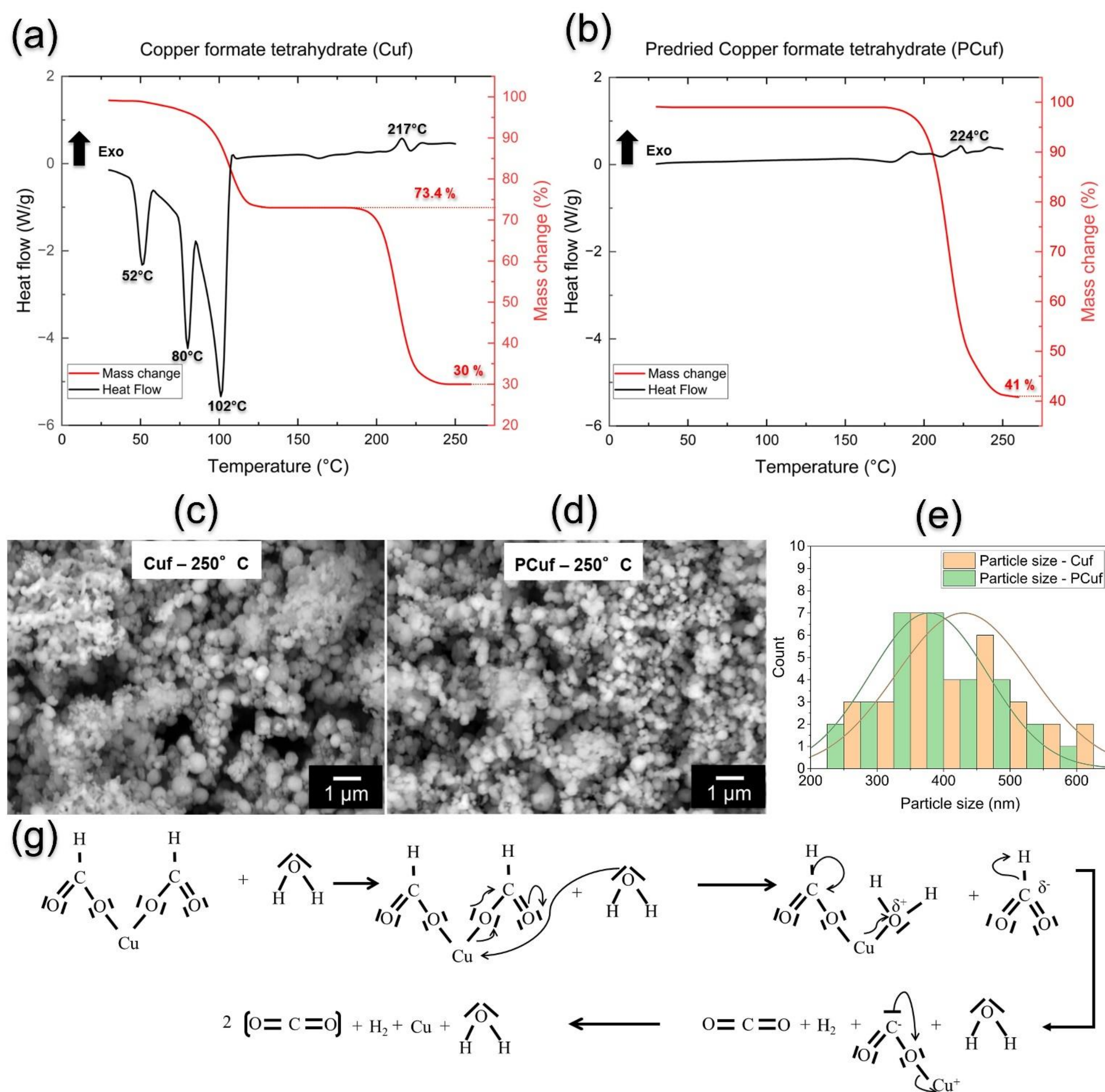


**Fig. 2** Fig. 1 DSC-TGA analysis highlighting peak exothermic and endothermic temperatures and % mass losses for Cuf (a) and PCuf (b), SEM images of Cuf (c) and PCuf (d) obtained after thermal decomposition at 250°C under $N_2$ without any isothermal holding time at 250°C to prevent further sintering of the particles, (e) Particle size distribution measured for Cuf and PCuf from the SEM images (c) and (d) respectively using Image J software, (g) Reaction mechanism showing the catalytic effect of water in the decomposition of Cu formate.[49]

Further, this can be elaborated by the following chemical reaction as seen in Fig. 3.d and Fig. 3.e. The difference of the chemical reaction of A2P and HA is due to the partial charge of the amine nitrogen. Primary amine groups are commonly electron donator because one lone pair electrons presence that are employed to link (ligand) both A2P and HA to Cu. This produces an electron deficiency of nitrogen owing to loses one electron on external orbital. The elements and group bonded with the nitrogen mitigates this positive partial charge via the donation of negative (electrons) charge. The hydrogens and carbon chain donate part of their negative charge to nitrogen for both inks because nitrogen is more electronegative. The capacity of the carbon chain to donor negative charge depends on various factors such as the length of the principal chain and the functional groups. Long principal chain can donate more negative charge than



Please do not adjust margins

Please do not adjust margins



short chain. The functional groups with more electronegative element usually reduce the carbon chain capacity to donate negative charge. Based on this fact, the difference in decomposition reaction between Cuf-A2P and Cuf-HA can be explained. A2P possessed a short carbon chain with alcohol group, which is more electronegative than carbon, while HA had a long carbon chain without functional group. Thus, A2P carbon chain donors have less negative charge to nitrogen that needs to compensate for this deficiency. The hydrogens bonded with nitrogen are the elements that donate their negative charges, increasing their electropositivity. This strengthens the link (ligand) between oxygen of the formate, which has a negative charge, and the hydrogen of the amine group. This promotes the breaking of the bond between formate oxygen and copper, prompting the decomposition of Cuf. Therefore, the decomposition process is faster in case of Cuf-A2P than Cuf-HA.

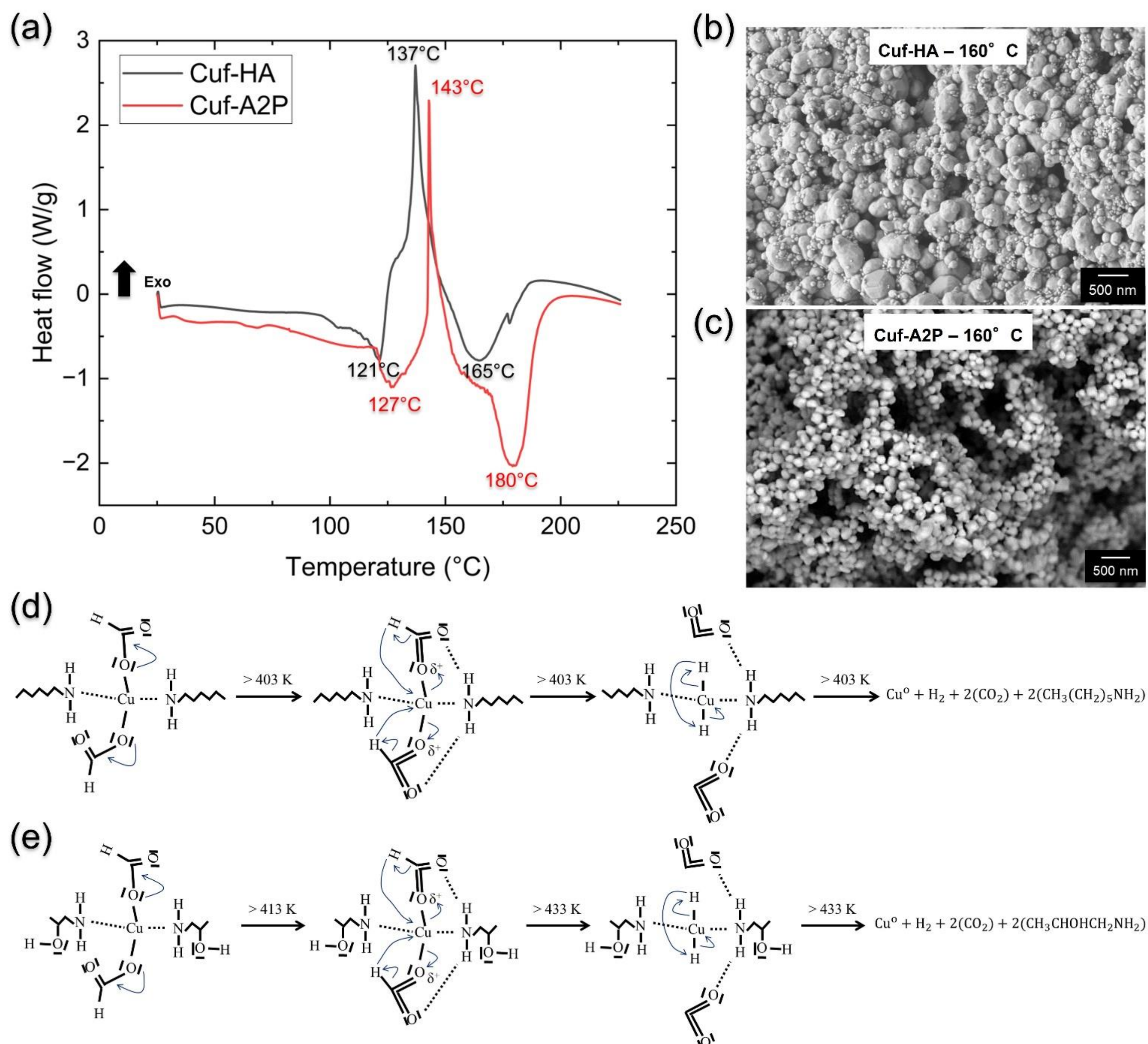


**Fig. 3** . (a) DSC analysis highlighting peak exothermic and endothermic temperatures for Cuf-HA and Cuf-A2P during the decomposition process of the amine complexes, SEM images of Cuf-HA (b) and Cuf-A2P (c) after decomposition at 160°C under $N_2$, without any isothermal holding at 160°C, (d) Decomposition reaction mechanism of Cuf – alkylamine (Cuf-HA)[21,51] , € Decomposition reaction mechanism of Cuf – alkanolamine (Cuf-A2P)[21,51].

### Decomposition mechanism and characterization of Cuf-A2P complexes based on different molar ratios

Alkanolamine complexes with Cuf in general are found to be soluble in alcohols. This is beneficial for preparation of printable low viscosity inks.[21] Therefore, in this case, A2P is considered to be a preferred complexing agent for the formulation of Cu complex inks. A2P bonds to Cu ions in a bidentate fashion, however the exact thermal decomposition mechanism of the complex is still unconfirmed. A further investigation is carried out to understand the decomposition

 This journal is © The Royal Society of Chemistry 20xx

Please do not adjust margins

Please do not adjust margins



mechanism of this complexing agent and the influence of molar ratio of Cuf to A2P on particle morphology. Fig. 4.a shows the DSC measurements of thermal decomposition of A2P and Cuf and A2P complexed in three mixing molar ratios 1:1, 1:2 and 1:3. Higher molar ratios were not investigated. This was done to reach a good compromise between the Cu metal content in the complex ink and the complete decomposition process.

From the DSC curve of pure A2P, green curve in Fig. 4.a, one obtains that the main evaporation (endothermic process) takes place between 130°C and 160°C. The endothermic peak is observed at 151°C, which is close to the boiling point of pure A2P (160°C). The decomposition of Cuf-A2P (1:2), in which the appropriate stochiometric relation is realized to form the complex, is depicted in the red curve of Fig. 4a. The flat decline of the DSC curve in the range of 100°C indicates the removal of water of hydration. The first endothermic peak indicates the dehydration process of the Cuf at 127°C. This behaviour also corresponds to the first mass loss observed in the TGA curves (Fig. 4b), where mass loss for 1:2 Cuf:A2P complex start at 90°C. The decomposition of Cuf-A2P complex comprises of the decarboxylation reaction and the removal of coordinated amine group from the Cu ion. The first exothermic peak indicates the start of the thermal decomposition process (formation of atomic Cu which aggregates to NP) of the Cuf-A2P complex where $CO_2$ and $H_2O$ is released after the dissociation of the carboxyl group that is weakly bonded to the Cu ion compared to the amine group.[31] For 1:2 Cuf-A2P complexes, the carboxyl dissociation starts at 140°C, where the exothermic peak is observed at 143°C. As the temperature increases to 160°C, an endothermic peak is observed at 178°C indicating the evaporation of A2P which is released due to the decomposition reaction.

Similar to Cuf-A2P (1:2), the DSC curve (black) for Cuf:A2P (1:1) (Fig. 4a) shows the first endothermic peak indicating the dehydration process. The endothermic peak for the dehydration process is observed at 122°C. The mass loss in this case starts at 70°C as observed in the TGA curve in Fig. 4b, which is similar to as seen in Cuf. For 1:1 Cuf-A2P complexes, the carboxyl dissociation starts also at 140°C, where an exothermic peak is observed at 148°C. However, the exothermic peak is smaller compared to 1:2 molar ratio indicating insufficient ligand formation between Cuf and A2P caused by the lower amount of A2P. In case of 1:1 Cuf-A2P complex, the endothermic contribution caused by A2P evaporation is significant smaller due to the lower amount of A2P and the overlapping broadened exothermic decomposition reaction and endothermic evaporation. An exothermic peak is also observed around 230°C indicating the decomposition of the excess Cuf that hasn't undergone ligand formation or complexing with A2P. From the TGA measurements (Fig. 4.b), it is observed that around 10% mass loss occurs after 200°C indicating the decomposition of the non-complexed Cuf.

The DSC curve (blue) for Cuf:A2P (1:3) in Fig. 4a shows no endothermic peak that can be assigned to the dehydration process. It is assumed that the dehydration temperature shifts to higher temperature close to the decomposition temperature. The first mass loss in case of 1:3 Cuf:A2P complex starts also at 90°C same as 1:2 Cuf-A2P complex (see Fig. 4.b). No pronounced exothermic peak for the decomposition of the complexed Cuf is visible. This can be attributed to the overlap of endothermic evaporation of the excess A2P that has not coordinated (no ligand formation) with the Cuf and the exothermic Cuf complex decomposition (decarboxylation reaction). A negative peak at 148°C (Fig. 4.a) indicates energy consumed during the endothermic reaction (evaporation of excess A2P) is greater than energy released during the exothermic reaction (decarboxylation reaction). For 1:3 Cuf-A2P complex, an endothermic peak at 148°C is observed which coincides with the endothermic peak observed during the evaporation of A2P (at 152°C). A third endothermic peak is observed for 1:3 Cuf-A2P complex at 176°C that occurs due to the evaporation of the released A2P by the decomposition of the Cuf complex as observed for 1:2 Cuf-A2P.

Fig. 4.c, 4.d and 4.e shows the SEM images for DSC samples after decomposition of 1:1, 1:2 and 1:3 Cuf-A2P complexes respectively. From the SEM images, it can be seen that larger crystalline structures with smaller Cu NPs are formed in case of complex with 1:1 molar ratio compared to the complexes with 1:2 and 1:3 molar ratios. This can be inferred from DSC and TGA curves, where the decomposition process was partially done by the complexing agent A2P and later the non-complexed Cuf crystals were decomposed forming larger Cu particles (as seen in Fig. 4.c). This two-step decomposition process also contributed to the growth and agglomeration of in-situ formed Cu NPs resulting in particles as large as 2-5 µm. Further, it is evident from the literature that recrystallization of non-complexed Cu salt in case of 1:1 Cuf-A2P can take place.[47-48] The water retained in the unreacted Cuf crystals during the decomposition process of Cu complex, can promote recrystallization of metastable water-depleted hydrate.[47-48] This could lead to formation of larger Cu formate crystals which upon decomposition form larger Cu particles (as seen in Fig. 4.c). Further, few Cu particles form a crystalline structure with distinct faces that can result from surface coordinating ligands or selective adsorption of the solvents on the surface of formed particles.[37] In Fig. 4.f and 4.g, the formed Cu particles are in the range of 100-500 nm. There is no difference in morphology between the nanostructures observed for 1:2 and 1:3 Cuf-A2P complexes. This infers that 1:2 Cuf-A2P molar ratio is sufficient for the decomposition of Cuf-A2P complex. In general, the formation and growth of Cu NPs in an ionic solution is a thermodynamic or kinetic driven process, which depends on the supersaturation and temperature of the complex solution.[37,40] This can be further influenced when additional solvents are added to the Cuf-A2P complex for preparation of Cu complex inks. Further trials are ongoing to control the growth of these in-situ formed Cu NPs via understanding the influence of solvent chemistry on the particle morphology. One can conclude from the analysis that a composition of 1:2 should be chosen to complex all Cuf but avoiding excess A2P that is not improving the process but solely reducing the metal content of the ink.

This journal is © The Royal Society of Chemistry 20xx



Please do not adjust margins

Please do not adjust margins



**Fig. 4 (** (a) DSC analysis highlighting peak exothermic and endothermic temperatures for Cuf-A2P complexes with molar ratio (1:1, 1:2 and 1:3) and A2P during the thermal decomposition process of the amine complexes, (b) TGA analysis showing mass loss (%) for Cuf-A2P complexes with molar ratio (1:1, 1:2 and 1:3) during the thermal decomposition process of the amine complexes, (c) SEM image of Cuf and A2P complexes with 1:1 molar ratio after decomposition at 250°C in the DSC chamber under $N_2$ at 10°C/min, (d) SEM image of Cuf and A2P complexes with 1:1 molar ratio after decomposition at 250°C in the DSC chamber under $N_2$ at 10°C/min, (e) SEM image of Cuf and A2P complexes with 1:1 molar ratio after decomposition at 250°C in the DSC chamber under $N_2$ at 10°C/min.

**Influence of solvent formulation on particle morphology in Cu complex inks**

In the earlier section, decomposition mechanism of Cuf – A2P complex was discussed. This complex will be used in the next section as conductive ink for realizing of metallic traces on polyimide for printed electronic application. There are two important requirements that need to be fulfilled to form the traces: Firstly, the ink viscosity must be adjusted to a range between 5-20 mPa.s for inkjet printing.[54] This can be done by using a low boiling point solvent such as ethanol, having a viscosity of 0.8911 mPa.s at 25°C.[55] Secondly, a high boiling point solvent is required which provides good wettability and stability to the ink by decreasing the evaporation rate while storage and printing process.[25] In this study, two chemicals (ethanol and EG) are chosen initially to form the Cu complex ink. The ink is inkjet printed to form the metallic Cu traces after the sintering. The two solvents are mixed in a mass ratio of 75:25, where the Cuf – A2P complex ink formed has a viscosity of 16 mPas. Fig. 5 shows the contact angle measurement of the complex ink with and without the carrier solvents on Cu and polyimide substrates. It can be observed that without the carrier solvent, the Cuf – A2P complex ink forms a contact angle in the range of 11°-13° on Cu substrate and 9°-10° on polyimide substrate.

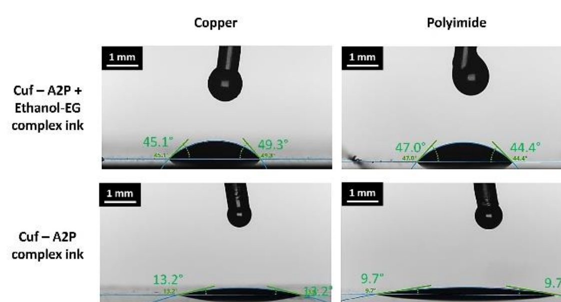


**Fig. 5** Contact angle measurement of the Cu complex ink with and without the carrier solvent (Ethanol + EG) on Cu and polyimide substrates.



This journal is © The Royal Society of Chemistry 20xx

Please do not adjust margins

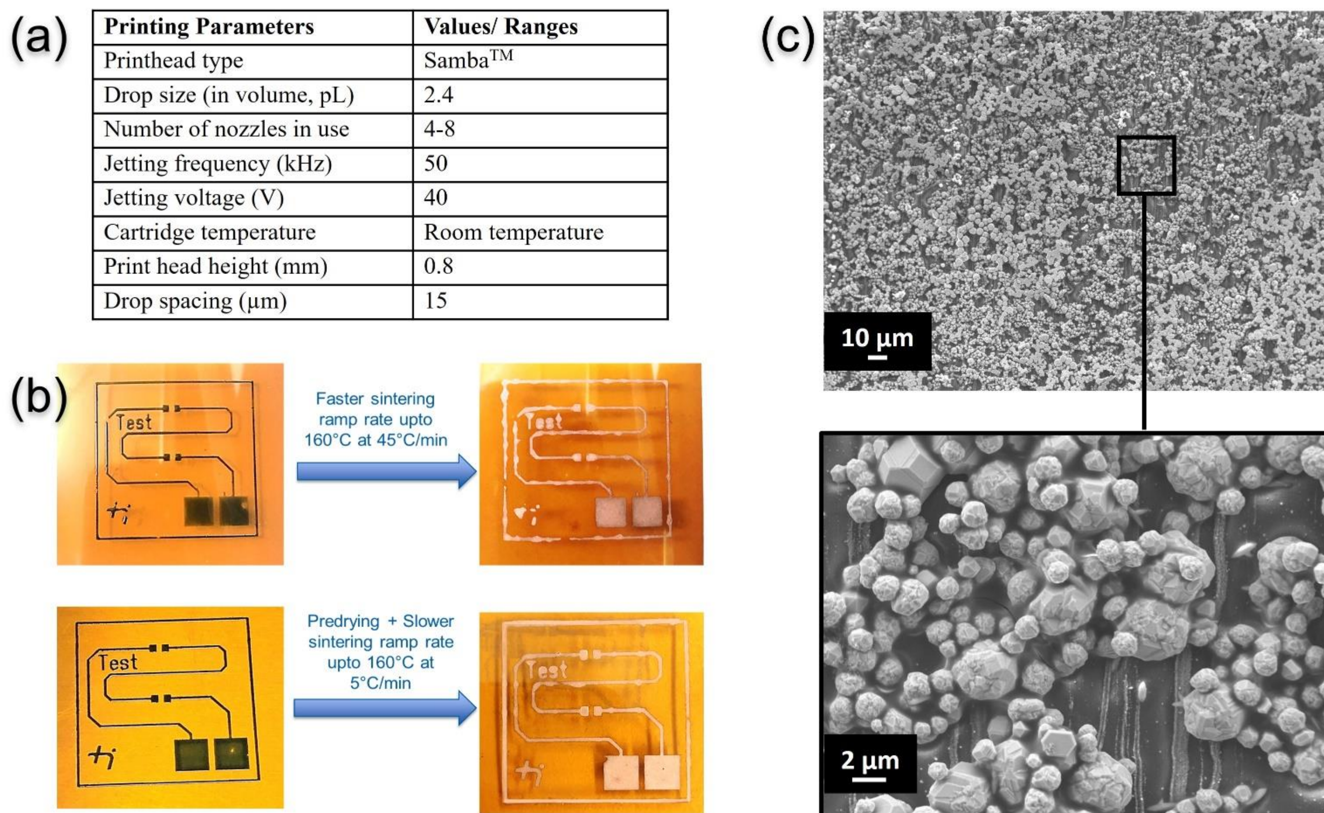

| Printing Parameters | Values/ Ranges |
|---|---|
| Printhead type | Samba™ |
| Drop size (in volume, pL) | 2.4 |
| Number of nozzles in use | 4-8 |
| Jetting frequency (kHz) | 50 |
| Jetting voltage (V) | 40 |
| Cartridge temperature | Room temperature |
| Print head height (mm) | 0.8 |
| Drop spacing (µm) | 15 |



**Fig. 6** Cu (II) formate tetrahydrate - A2P complex ink inkjet printed onto the polyimide substrate. (a.) Inkjet printing parameters for printing the Cu complex ink. (b) Printed pattern before and after the sintering process utilizing faster sinter ramp rate (top) and predrying + slower ramp rate (bottom). (c) SEM images of the particles formed after predrying + slower ramp rate sintering process, (top) lower magnification and (bottom) higher magnification.

In order to achieve a printed pattern with good aspect ratio and resolution, the preferred contact angle should be in the range of 40°-50°. Using the carrier solvent with ethanol and EG in the Cuf – A2P complex, the given range is achieved for both the Cu and polyimide substrate. Based on these two requirements, a Cu complex ink formulation is made having a Cu metal content of 6.95 wt.%.

The prepared Cu complex ink is then printed using the inkjet printer on a polyimide substrate using the printing parameters as shown in Figure 6.a. After printing, a pre-drying step is necessary for Cu complex inks, as they undergo high volume shrinkage due to high organic content (>90 wt. %).[25] The rapid evaporation of these organics causes problems such as distortion of printed pattern due to formed bubbles, uneven spreading of the printed traces (coffee ring effect) and surface cracking.[56] For this, an efficient degassing process, reported to tackle the challenges of rapid bubbling during the decomposition of Cu complex inks using a pre-drying and slow ramp rate sintering step (as seen in Figure 6.b)[25] was implemented. Due to slower ramp rate (5°C/ min) of the sintering process, larger particles were formed resulting in sparse distribution of particles in the entire trace contributing to a poor bulk resistivity of 102 µΩcm. Figure 6.c shows the SEM images of the particles formed after this slow ramp rate sintering process. It should be noted that after the synthesis of the Cu complex ink with carrier solvents for inkjet printing, the Cu metal content (in wt.%) in the ink decreases from 21.08 to a mere 6.95 wt.%. SEM images shows that larger particle agglomerates ranging from 2-5 µm are formed as result of slower ramp rate. The decomposition process of Cuf-A2P complex starts at ~127°C as seen in the DSC (Fig. 3.a) by dissociation of the carboxyl group (Fig. 3.e). The nucleation process starts with the formation of Cu nuclei followed by growth into Cu nanoparticles at 130°C as seen in the Fig. 7.a.[52] Additionally, it is reported that the released amine ligand restricts the growth of Cu nanoparticles because it forms secondary bonds with the copper and hinders the copper crystal growth.[57-58] This is phenomenon observed in the inks investigated in this study since the removal of amine ligands is observed to start at ~ 165°C as observed by the DSC (Fig. 3.a). Therefore, a significant growth of Cu nanoparticles from 30-50 nm at 130°C to 100-200 nm at 180°C is observed (as seen in Fig. 7.a).

During the slower heating ramp rate process (5°C/min), the nanoparticles formed have sufficient time to migrate and reduce their surface energy through surface diffusion during sintering process. This process leads to formation of larger aggregates as smaller particles fuse or adhere to each other(coalescence). Another mechanism, which can take place is Ostwald ripening – a phenomenon where larger particles grow at expense of smaller particles.[59] This reduces the number of solid particles formed in the entire trace until the bulk solution reaches an equilibrium state.[60] Additionally, faster ramp rates (45°C/ min) may contribute to reduced growth of particles, enabling formation of finer particles. However, it is observed that rapid evaporation of organics during sintering of Cu complex caused bubbling resulting in discontinuous traces.

In order to solve this issue, various surfactants or capping agents are considered in conventional NP synthesis process to control the



Please do not adjust margins
Please do not adjust margins

Please do not adjust margins



growth of NPs. These stabilizing agents reduce the surface energy of the formed NP with selectively adsorbing onto the surface preventing aggregation/ agglomeration in the solution state.[37-38] Based on this concept, PEG 600 was added to the complex ink at very low concentration (ranging from 0.5 -1 wt.% of the ink). Figure 7.a shows the decomposition process schematic of the Cu complex ink with PEG 600. To facilitate efficient removal of PEG 600 from the system, a vacuum process was integrated at 250°C for 1 minute. Figure 7.b shows the SEM images of Cu particles formed after the sintering process with an additional vacuum step. From this study, it was clear that PEG 600 prevented the aggregation/agglomeration of NPs and effectively controlled the size and shape of in-situ generated Cu NPs. The newly synthesized Cu complex ink with PEG 600 showed reliable results both in terms of printability and sinterability. The bulk resistivity of the Cu metallic trace obtained on the polyimide substrate after 5 layers of printing, sintered at 250°C for 5 minutes under nitrogen was 20.48 μΩcm. This is only 12 times that of bulk resistivity of pure Cu. These results show that using simple chemical approaches to control the size of the in-situ generated Cu NPs, homogenous and densely packed sintered Cu metallic structure can be obtained for fabrication of devices for printed electronics application. Further investigations are ongoing to understand the mechanism by which PEG600 as well other size controlling binder interact with the *in-situ* formed Cu NPs.

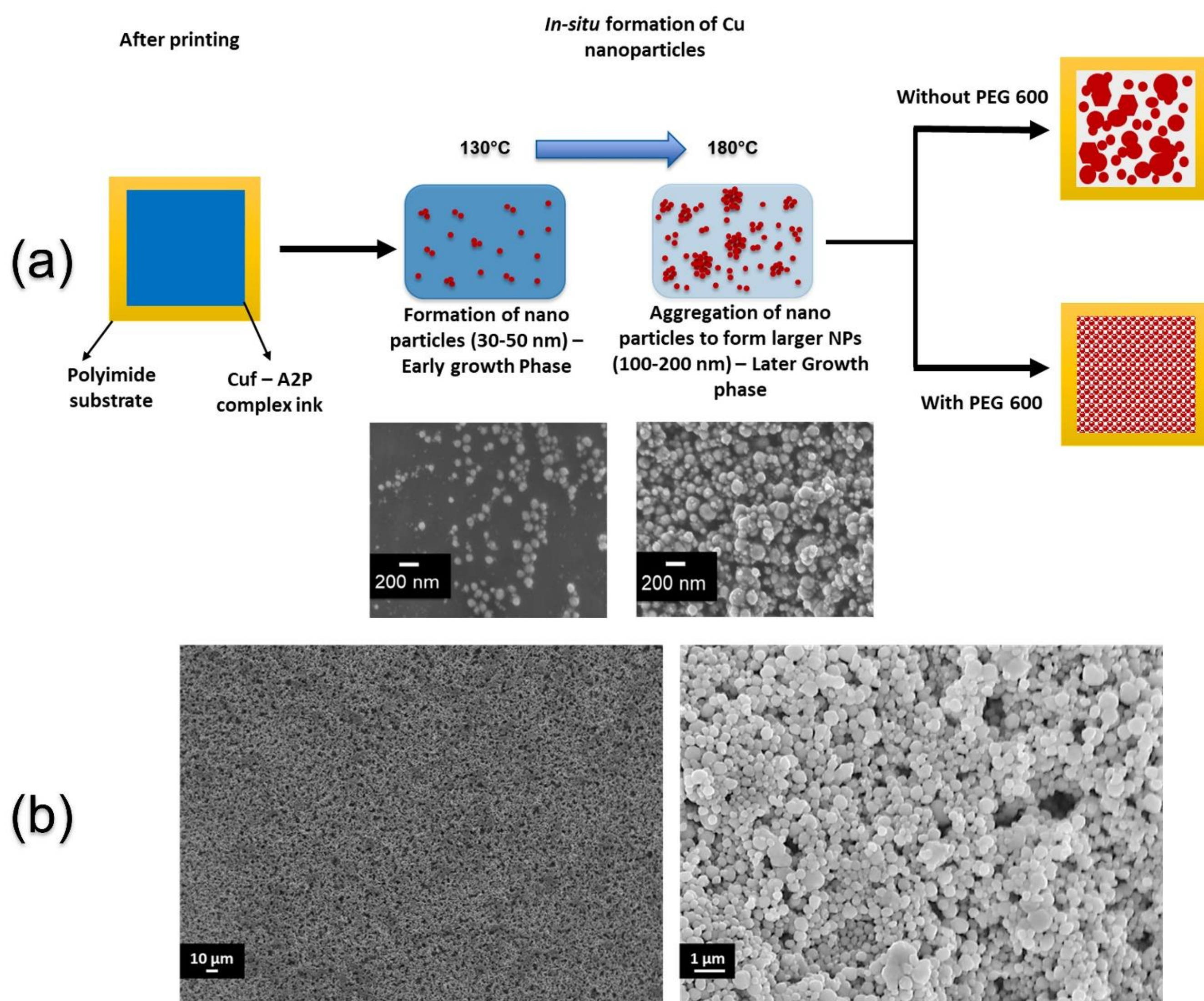


**Fig. 7** (a.) Schematic of *in-situ* formation of Cu nanoparticles after decomposition of Cu complex ink with and without PEG 600. (b) SEM images of Cu particles formed after sintering at 250°C for 5 minutes under $N_2$ with an additional vacuum step (at the start of isothermal holding time for 1 minute), where (left image) – lower magnification and (right image) – higher magnification.

## Conclusions

In this study, various approaches were employed, ranging from understanding the decomposition mechanism of Cuf to the influence of binder formulation, to synthesize Cu complex inks and observe their effects on the morphology of in-situ generated Cu NPs. Water of hydration in Cuf acts as a catalysing agent lowering the decomposition temperature of Cuf compared to PCuf as observed in the DSC. From the



This journal is © The Royal Society of Chemistry 20xx

Please do not adjust margins

Please do not adjust margins



decomposition mechanism of Cuf-A2P and Cuf-HA, it is found that the decomposition reaction is faster in case of Cuf-A2P than Cuf-HA leading to formation of smaller NPs. This is attributed to two reasons: Firstly, the carbon chain is smaller in case of A2P than HA, therefore the primary carbon is less electronegative making the nitrogen also less electronegative, thus releasing the hydrogen atom earlier from the amine group. Secondly, the alcohol group in alkanolamine also reduces the primary carbon electronegativity – therefore providing a catalysing effect in the decomposition reaction. Additionally, A2P provided good solubility to low boiling point alcohol solvents. By varying molar ratios of Cuf:A2P (1:1, 1:2 and 1:3), it is found that 1:2 molar ratio between Cuf and A2P is sufficient without further decreasing the Cu metal content in the Cuf-A2P complex and enables a complete decomposition compared to 1:1 molar ratio. For preparation of Cu complex inks, the rheological properties of the binder formulation needed to be carefully tailored with Cuf-A2P complex for successful preparation of Cu complex ink for printed electronic applications. During the sintering process, the impact of faster ramp rate and slower ramp rate was also investigated. Faster ramp rate contributed to reduced growth of particles, enabling formation of finer particles. However, rapid evaporation of organics during sintering of Cu complex caused bubbling resulting in discontinuous traces. Slower ramp rate resulted in formation of larger particle aggregates (2-5 µm), since particles formed have sufficient time to diffuse with each other and form larger aggregates either by coalescence or Ostwald ripening. The incorporation of a small amount of PEG 600 as a particle stabilizing agent during the ink synthesis played a critical role. It effectively prevented the aggregation of NPs, ensuring the desired size and shape control of the in-situ generated Cu NPs. This strategy significantly enhanced the stability and performance of the Cu complex ink, paving the way for improved properties and potential applications in printed electronics. The novel formulation with PEG 600 resulted in a significant improvement in bulk resistivity, achieving a value of 20.48 µΩcm, representing a more than 400% improvement compared to the previous formulation without size controlling effects. In conclusion, the synthesis and optimization of Cu complex inks, along with the careful control of sintering parameters and the addition of stabilizing agents, proved to be crucial in achieving desirable morphology and electrical properties for printed electronic applications.

## Author Contributions

Nihesh Mohan: Conceptualization, Data curation, Formal Analysis, Investigation, Methodology, Project administration Software, Validation, Visualization, Writing – original draft, Writing – review & editing.

Sri Krishna Bhogaraju: Conceptualization, Formal Analysis, Investigation, Methodology, Project administration, Resources, Supervision, Validation, Review & editing.

Juan Ignacio Ahuir-Torres: Formal Analysis, Investigation, Methodology, Software, Supervision, Validation, Visualization, Writing – review & editing.

Ralf Webler: Investigation, Resources, Writing – review & editing.

Hiren Kotadia: Formal Analysis, Methodology, Supervision, Validation, Writing – review & editing.

Huseyin Erdogan: Resources, Writing – review & editing.

Gordon Elger: Conceptualization, Funding acquisition, Methodology, Project administration, Resources, Scientific Supervision, Validation, Writing – review & editing.

## Conflicts of interest

There are no conflicts to declare.

## Acknowledgements

The work was financially supported by the Bavarian Collaborative Research Program (BayVFP) of the Free State of Bavaria, Germany within the project ‘‘ADDIRA’’ under the grant number DIE-2107-005//DIE0159/01. The authors thank Maxim Hiersig at Conti Temic Microelectronic GmbH (Ingolstadt) for help with the DSC measurements, Prof. Ulrich Tetzlaff (THI) and Dr. Georges Lemos (THI) for the SEM measurements.

## References

1 K. Sugunuma, New York: Springer, 2014.
2 V. Beedasy and P. J. Smith, Materials-MDPI, vol. 13, no. 704, 2020.
3 E. Ragonese, M. Fattori and E. Cantatore, IEEE Transactions on Circuits and Systems II: Express Briefs, vol. 68, no. 1, pp. 42-48, 2021.
4 W. Yang, X. Cheng, Z. Guo, Q. Sun, J. Wang and C. Wang, Journal of Materials Chemistry C, vol. 11, no. 2, pp. 406-425, 2023.
5 L. Grande, V. T. Chundi, D. Wei, C. Bower, P. Andrew, and T. Ryhänen, "Graphene for energy harvesting/storage devices and printed electronics," Particuology, vol. 10, no. 1, pp. 1-8, 2012.
6 M. Hosseini, M. Javad, and R. A. Nawrocki, "A review of the progress of thin-film transistors and their technologies for flexible electronics," Micromachines, vol. 12, no. 6, p. 655, 2021.
7 Y. Khan, A. Thielens, S. Muin, J. Ting, C. Baumbauer and A. C. Arias, "A new frontier of printed electronics: flexible hybrid electronics," Advanced Materials, vol. 32, no. 15, p. 1905279, 2020.
8 S. Khan, S. Ali and A. Bermak, "Recent Developments in Printing Flexible and Wearable Sensing Electronics for Healthcare Applications," Sensors, vol. 19, no. 5, p. 1230, 2019.
9 G. Kuczynski, "Self-Diffusion in Sintering of Metallic Particles," in Sintering Key Papers, Dordrecht, Springer Netherlands, 1990, pp. 509-527.



Please do not adjust margins

Please do not adjust margins




10 H. Tan, J. An, C. Chua and T. Tran, "Metallic nanoparticle inks for 3D printing of electronics," Advanced Electronic Materials, vol. 5, no. 5, p. 1800831, 2019.
11 K. Rajan, I. Roppolo, A. Chiappone, S. Bocchini, D. Perrone and A. Chiolerio, "Silver nanoparticle ink technology: state of the art.," Nanotechnology, science and applications , pp. 1-13, 2016.
12 L. Mo, G. Zhenxin, Y. Li, Z. Qingqing, Y. Fang and et al., "Silver nanoparticles-based ink with moderate sintering in flexible and printed electronics," International journal of molecular sciences, vol. 20, no. 9, p. 2124, 2019.
13 J. Kang, H. Kim, J. Ryu, H. Hahn, S. Jang and J. Joung, "Inkjet printed electronics using copper nanoparticle ink," Journal of Materials Science: Materials in Electronics, vol. 21, pp. 1213-1220, 2010.
14 P. Karthik and S. Singh, "Copper conductive inks: synthesis and utilization in flexible electronics," RSC advances, vol. 5, no. 79, pp. 63985-64030, 2015.
15 W. Li, Q. Sun, L. Li, J. Jiu, X.-Y. Liu and M. Kanehara, "The rise of conductive copper inks: challenges and perspective," Applied Materials Today, vol. 18, no. 100451, 2019.
16 Y. Choi, K.-d. Seong and Y. Piao, "Metal–Organic Decomposition Ink for Printed Electronics," Adv. Mater. Interfaces, Vols. 6, 1901002, 2019.
17 W. Yang, E. J. L. Kratochvil and C. Wang, "Metal particle free inks for printed flexible electronics," J. Mater. Chem. C. , vol. 7, no. 15098, 2019.
18 Y. Farraj, M. Grouchko and S. Magdassi, "Self-reduction of a copper complex MOD ink for inkjet printing conductive patterns on plastics," Chemical Communications, vol. 51, no. 9, pp. 1587-1590, 2015.
19 D.-H. Shin and Et-al., "A Self-Reducible and Alcohol-Soluble Copper-Based Metal–Organic Decomposition Ink for Printed Electronics," ACS Applied Materials & Interfaces, vol. 6, no. 5, pp. 3312-3319, 2014.
20 A. Yabuki, S. Kawahara, S. Kang and I. W. Fathona, "Low-temperature synthesis of copper conductive film by thermal decomposition of copper–amine complexes with a low boiling point," Thin Solid Films, vol. 519, no. 19, pp. 6530-6533, 2020.
21 C. Paquet, T. Lacelle, X. Liu, B. Deore and A. J. Kell, "The role of amine ligands in governing film morphology and electrical properties of copper films derived from copper formate-based molecular inks," Nanoscale, no. 10, pp. 6911-6921, 2018.
22 A. Yabuki, A. Norzafriza and M. Yanase, "Low-temperature synthesis of copper conductive film by thermal decomposition of copper–amine complexes," Thin Solid Films, vol. 519, no. 19, pp. 6530-6533, 2011.
23 T. Yonezawa, H. Tsukamoto, Y. Yong, M. T. Nguyen and M. Matsubara, "Low temperature sintering process of copper fine particles under nitrogen gas flow with Cu2+-alkanolamine metallacycle compounds for electrically conductive layer formation," RSC Advances, vol. 6, no. 15, pp. 12048-12052, 2016.
24 B. Zhang, C. Chen, W. Li, J. Yeom and K. Suganuma, "Well-Controlled Decomposition of Copper Complex Inks Enabled by Metal Nanowire Networks for Highly Compact," Conductive, and Flexible Copper Films, vol. 7, no. 1, p. 1901550, 2020.
25 N. Mohan, R. Saccon, S. K. Bhogaraju and G. Elger, "Cu complex inks for printed electronics application-challenges and solutions," in Mikro-Nano-Integration; 9. GMM-Workshop, Aachen, Germany, 2022.
26 Martinez de la Torre, C., Grossman, J. H., Bobko, A. A., & Bennewitz, M. F. (2020). Tuning the size and composition of manganese oxide nanoparticles through varying temperature ramp and aging time. *PLoS One*, *15*(9), e0239034.
27 Kim, S. J., Lee, J., Choi, Y. H., Yeon, D. H., & Byun, Y. (2012). Effect of copper concentration in printable copper inks on film fabrication. Thin Solid Films, 520(7), 2731-2734.
28 Wang, B. Y., Yoo, T. H., Song, Y. W., Lim, D. S., & Oh, Y. J. (2013). Cu ion ink for a flexible substrate and highly conductive patterning by intensive pulsed light sintering. ACS applied materials & interfaces, 5(10), 4113-4119.
29 Yabuki, A., & Tanaka, S. (2012). Electrically conductive copper film prepared at low temperature by thermal decomposition of copper amine complexes with various amines. Materials Research Bulletin, 47(12), 4107-4111.
30 Rosen, Y., Grouchko, M., & Magdassi, S. (2015). Printing a Self-Reducing Copper Precursor on 2D and 3D Objects to Yield Copper Patterns with 50% Copper's Bulk Conductivity. Advanced Materials Interfaces, 2(3), 1400448.
31 Xu, W., & Wang, T. (2017). Synergetic effect of blended alkylamines for copper complex ink to form conductive copper films. Langmuir, 33(1), 82-90.
32 Farraj, Y., Layani, M., Yaverboim, A., & Magdassi, S. (2018). Binuclear copper complex ink as a seed for electroless copper plating yielding> 70% bulk conductivity on 3D printed polymers. Advanced Materials Interfaces, 5(8), 1701285.
33 Kwon, Y. T., Kim, Y. S., Lee, Y., Kwon, S., Lim, M., Song, Y., ... & Yeo, W. H. (2018). Ultrahigh conductivity and superior interfacial adhesion of a nanostructured, photonic-sintered copper membrane for printed flexible hybrid electronics. ACS applied materials & interfaces, 10(50), 44071-44079.
34 Kang, S., Tasaka, K., Lee, J. H., & Yabuki, A. (2021). Self-reducible copper complex inks with two amines for copper conductive films via calcination below 100° C. Chemical Physics Letters, 763, 138248.
35 Yabuki, A., Kawahara, S., Kang, S., & Fathona, I. W. (2020). Low-temperature synthesis of copper conductivity film from a copper formate amine complex with a low boiling point. Materials Science and Engineering: B, 262, 114743.
36 Shabanov, N. S., Rabadanov, K. S., Suleymanov, S. I., Amirov, A. M., Isaev, A. B., Sobola, D. S., ... & Asvarova, G. A. (2021). Water-soluble copper ink for the inkjet fabrication of flexible electronic components. Materials, 14(9), 2218.
37 Z. Wu, S. Yang and W. Wu, "Shape control of inorganic nanoparticles from solution," Nanoscale, vol. 8, no. 3, pp. 1237-1259, 2016.
38 D. Mott, J. Galkowski, L. Wang, J. Luo and C. J. Zhong, "Synthesis of size controlled and shaped copper nanoparticles," Langmuir, vol. 23, no. 10, pp. 5740-5745, 2007.
39 M. A. Ben Aissa, B. Tremblay, A. Andrieux-Ledier, E. Maisonhaute, N. Raouafi and A. Courty, "Copper nanoparticles of well-controlled size and shape: a new advance in synthesis and self-organization," Nanoscale, vol. 7, no. 7, pp. 3189-3195, 2015.
40 C. Wei and L. Qiming, "Shape-, size-, and density-tunable synthesis and optical properties of copper nanoparticles," CrystEngComm, vol. 19, no. 24, pp. 3254-3262, 2017.
41 H. Kawasaki, Y. Kosaka, Y. Myoujin, T. Narushima, T. Yonezawa and R. Arakawa, "Microwave-assisted polyol synthesis of copper nanocrystals without using additional protective agents," Chemical Communications, vol. 47, no. 27, pp. 7740-7742, 2011.
42 F. Dimatix, "FUJIFILM Dimatix Materials Printer DMP 2850 User Manual," 2016.
43 Gutiérrez, M. P., Li, H., & Patton, J. (2002). Thin film surface resistivity. Materials Engineering, 0-24.
44 Heyns, A. M., & Range, K. J. (1987). The vibrational spectra of the copper (II) formates: Part IV. The thermal behaviour of Cu (HCOO) 2· 4H2O and Cu (HCOO) 2· 2H2O. Journal of Molecular Structure, 162(1-2), 57-67.



This journal is © The Royal Society of Chemistry 20xx

Please do not adjust margins

Please do not adjust margins



45 Choi, Y. H., Lee, J., Kim, S. J., Yeon, D. H., & Byun, Y. (2012). Highly conductive polymer-decorated Cu electrode films printed on glass substrates with novel precursor-based inks and pastes. Journal of Materials Chemistry, 22(8), 3624-3631.
46 Dong, Y., Lin, Z., Li, X., Zhu, Q., Li, J. G., & Sun, X. (2018). A low temperature and air-sinterable copper–diamine complex-based metal organic decomposition ink for printed electronics. Journal of Materials Chemistry C, 6(24), 6406-6415.
47 Fichte, P. M., & Flanagan, T. B. (1971). Kinetics of dehydration of single crystals of copper formate tetrahydrate. Transactions of the Faraday Society, 67, 1467-1479.
48 Galwey, A. K. (2000). Structure and order in thermal dehydrations of crystalline solids. Thermochimica acta, 355(1-2), 181-238.
49 Pascher, T. F., Ončák, M., van der Linde, C., & Beyer, M. K. (2019). Release of Formic Acid from Copper Formate: Hydride, Proton-Coupled Electron and Hydrogen Atom Transfer All Play their Role. ChemPhysChem, 20(11), 1420-1424.
50 Paquet, C., Lacelle, T., Deore, B., Kell, A. J., Liu, X., Korobkov, I., & Malenfant, P. R. L. (2016). Pyridine–copper (II) formates for the generation of high conductivity copper films at low temperatures. Chemical communications, 52(12), 2605-2608.
51 Shin, H., Liu, X., Lacelle, T., MacDonell, R. J., Schuurman, M. S., Malenfant, P. R., & Paquet, C. (2020). Mechanistic insight into bis (amino) copper formate thermochemistry for conductive molecular ink design. ACS applied materials & interfaces, 12(29), 33039-33049.
52 Shrestha, S., Wang, B., & Dutta, P. (2020). Nanoparticle processing: Understanding and controlling aggregation. Advances in colloid and interface science, 279, 102162.
53 Liu, J., Lv, W., Mou, Y., Chen, C., & Kang, Y. (2023). Coalescence behavior of Cu nanoparticles during sintering: Based on atomic scale to macro scale. Journal of Materials Research and Technology, 27, 2490-2507.
54 Lejeune, M., Chartier, T., Dossou-Yovo, C., & Noguera, R. (2009). Ink-jet printing of ceramic micro-pillar arrays. Journal of the European Ceramic Society, 29(5), 905-911.
55 Tanaka, Y., Yamamoto, T., Satomi, Y., Kubota, H., & Makita, T. (1977). Specific volume and viscosity of ethanol-water mixtures under high pressure. The Review of Physical Chemistry of Japan, 47(1), 12-24.
56 Kim, C., Nogi, M., & Suganuma, K. (2012). Electrical conductivity enhancement in inkjet-printed narrow lines through gradual heating. Journal of Micromechanics and Microengineering, 22(3), 035016.
57 Choi, Y. H., & Hong, S. H. (2015). Effect of the Amine concentration on phase evolution and densification in printed films using Cu (II) complex ink. Langmuir, 31(29), 8101-8110.
58 Sun, Z. H., Oyanagi, H., Nakamura, H., Jiang, Y., Zhang, L., Uehara, M., ... & Maeda, H. (2010). Ligand effects of amine on the initial nucleation and growth processes of CdSe nanocrystals. The Journal of Physical Chemistry C, 114(22), 10126-10131.
59 Liu, J., Lv, W., Mou, Y., Chen, C., & Kang, Y. (2023). Coalescence behavior of Cu nanoparticles during sintering: Based on atomic scale to macro scale. Journal of Materials Research and Technology, 27, 2490-2507.
60 Cao, G. (2004). Nanostructures & nanomaterials: synthesis, properties & applications. Imperial college press.

This journal is © The Royal Society of Chemistry 20xx



Please do not adjust margins